

# Efficient Registration of Forest Point Clouds by Global Matching of Relative Stem Positions

Xufei Wang, Zexin Yang, Xiaojun Cheng, Jantien Stoter, Wenbin Xu, Zhenlun Wu, and Liangliang Nan

**Abstract**—Registering point clouds of forest environments is an essential prerequisite for LiDAR applications in precision forestry. State-of-the-art methods for forest point cloud registration require the extraction of individual tree attributes, and they have an efficiency bottleneck when dealing with point clouds of real-world forests with dense trees. We propose an automatic, robust, and efficient method for the registration of forest point clouds. Our approach first locates tree stems from raw point clouds and then matches the stems based on their relative spatial relationship to determine the registration transformation. In contrast to existing methods, our algorithm requires no extra individual tree attributes and has linear complexity to the number of trees in the environment, allowing it to align point clouds of large forest environments. Extensive experiments have revealed that our method is superior to the state-of-the-art methods regarding registration accuracy and robustness, and it significantly outperforms existing techniques in terms of efficiency. Besides, we introduce a new benchmark dataset that complements the very few existing open datasets for the development and evaluation of registration methods for forest point clouds.

**Index Terms**—Point cloud, registration, forest, laser scanning, dataset.

## I. INTRODUCTION

THE light detection and ranging (LiDAR) technology, especially terrestrial laser scanning (TLS), has brought forest inventories to a brand new 3D era [1]–[3]. The registration of TLS scans collected from different viewpoints is a fundamental and necessary precondition for subsequent forestry applications. However, the registration of forest point clouds remains a challenging task due to the mutual occlusion of forest structures. The most common and reliable practice is marker-based registration, which requires manually placing and transporting markers and is thus expensive, laborious,

and time-consuming. Approaches dedicated to urban scenes rely on either local [4], [5] or global [6] descriptors, which are effective for well-structured urban environments. However, due to the complexity, irregularity, and instability of forest environments, these methods become fragile and ineffective when applied to forest point clouds.

Given the fact that tree stems are the most stable structure in the forest environment, existing forest point cloud registration methods rely on the extracted tree stems and other attributes for the registration. These methods share a similar two-stage workflow: *stem mapping* followed by *stem matching* [7]–[18]. The stem mapping stage locates tree stem positions and extracts necessary individual tree attributes, e.g., diameter at breast height (DBH) and tree height. The second stage establishes correspondences of tree stems across a pair of point clouds by matching their positions and attributes, which is typically conducted in an iterative trial-and-error manner (see Fig. 1 (a)). Although this stem-based strategy has been continuously improved in the past decades, significant limitations remain as follows.

1) *Inefficiency in stem mapping*. Most methods [9]–[13], [16], [17] adopt an existing algorithm originally developed for tree detection or parameter estimation to identify tree stems. However, the existing stem detection algorithms [19]–[25] can be time-consuming since they introduce computationally intensive steps (e.g., individual tree segmentation, leaf and wood separation, and subsection stem modeling) to guarantee the completeness of detection and the high accuracy of extracted tree attributes.

2) *Ambiguities and inefficiency in stem matching*. Most existing stem matching methods rely on both tree locations and other attributes (e.g., DBH, tree height, or tree crown) [10]–[15], [18], [26], and thus they are sensitive to ambiguities in the extracted tree attributes. For example, it is common that multiple trees in a plantation forest have similar DBH and height values. Besides, the overwhelming computational burden is a fatal flaw of most stem-based matching algorithms. Specifically, their running time grows dramatically with the increasing number of trees due to the exhaustive nature of their verification based on the iterative trial-and-error alignment framework, which results in their inability to handle forest data containing a large number of trees, not to mention the demand for highly accurate tree attributes.

3) *Insufficient data for evaluation*. Though improvements have been reported, the actual progress is vague to the research community because experiments are conducted on different closed datasets. To enable reliable evaluation and comparison of forest point cloud registration methods, open-access bench-

Manuscript received XX; revised XX; accepted XX. This work was funded by the National Natural Science Foundation of China (No. 41974213). Zexin Yang is supported by the China Scholarship Council (*Corresponding author: Zexin Yang*).

X. Wang is with the College of Surveying and Geo-Informatics, Tongji University, Shanghai 200092, China (email: tjwangxufei@tongji.edu.cn).

Z. Yang is with the College of Surveying and Geo-Informatics, Tongji University, Shanghai 200092, China, and also with the 3D Geoinformation Research Group, Delft University of Technology, 2628 BL Delft, The Netherlands (email: zexinyang@tongji.edu.cn).

X. Cheng was with the College of Surveying and Geo-Informatics, Tongji University, Shanghai 200092, China. He unfortunately passed away before the submission of this paper.

J. Stoter and L. Nan are with the 3D Geoinformation Research Group, Delft University of Technology, 2628 BL Delft, The Netherlands (email: j.e.stoter@tudelft.nl, liangliang.nan@tudelft.nl).

W. Xu is with the College of Environment and Resources, Zhejiang A&F University, Hangzhou 311300, China.

Z. Wu is with the Big Data Development Administration of Yichun, Yichun 336000, China.

mark datasets with a large data volume and diverse forestry scenarios are urgently needed but unfortunately lacking.

In this work, we aim to resolve the above bottlenecks to achieve efficient and robust registration of forest point clouds. Since exploiting individual tree attributes not only slows down stem mapping but also makes stem matching sensitive to the great complexity of forest environments, we build an efficient attribute-free registration method named *AlignTree* for forest point clouds. The proposed approach relies on tree positions only, avoiding the computationally expensive and unstable tree attribute derivation process. It consists of a stem mapping algorithm that can efficiently locate tree stems in raw scans and a simple yet significantly efficient stem matching algorithm that needs no extra tree attributes but only stem positions. Moreover, unlike most existing forest registration methods that follow the iterative trial-and-error procedure [7]–[16], [18], [26], [27] and have cubic or exponential complexity to the number of trees [9], [11], [13] or keypoints [14], [27], our work falls in the inlier-grouping framework, and it can establish the correspondence between two scans based on the relative positions of the trees. The comparison of these two frameworks is illustrated in Fig. 1. Our stem matching algorithm has linear complexity and thus can be applied to point clouds of large forest environments or those with dense tree instances. The proposed method inherits the effectiveness and robustness and meanwhile exceedingly increases the efficiency of the stem-based registration scheme.

Extensive experiments show that our approach significantly outperforms state-of-the-art methods in terms of efficiency, accuracy, and robustness. For comprehensive evaluation and valid comparison of registration algorithms, we also introduce a new benchmark dataset named *Tongji-Trees*, to complement the very rare publicly available data for marker-free registration of TLS scans of forest areas. In summary, our main contributions include<sup>1</sup>:

- 1) A fast stem mapping method that can robustly extract stem positions from raw forest scans.
- 2) A robust, efficient, and deterministic stem matching algorithm that requires only stem position information, which is suitable for registering point clouds of forestry scenes with a large number of trees.
- 3) A benchmark dataset for evaluating forest point cloud registration methods. The new dataset consists of twenty point clouds collected from four forest plots with diversity concerning understory vegetation and the density, distributions, and species of trees.

## II. RELATED WORK

In light of the extensive literature on point cloud registration [28], [29], in this section, we mainly review the works that are most relevant to ours, namely, stem mapping, stem-based registration, and benchmark datasets.

<sup>1</sup>The source code of *AlignTree* and the *Tongji-Trees* dataset will be made publicly available after the acceptance of the paper.

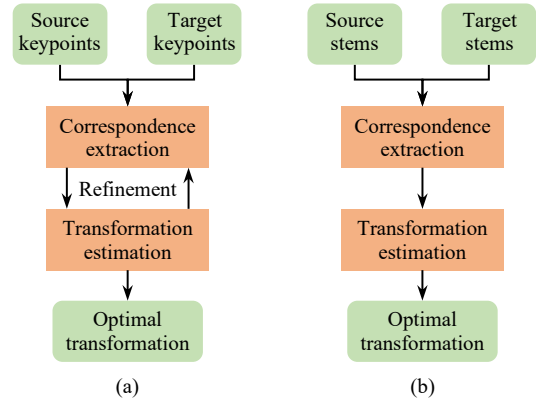


Fig. 1. Comparison between the existing forest point cloud registration framework and ours. (a) The iterative trial-and-error framework. Given two sets of keypoints, correspondences and transformations are estimated and refined iteratively until the optimal transformation is found. (b) Our inlier-grouping framework. With two sets of stem positions extracted from forest scans, our method first establishes correspondences by grouping all inliers, and then it computes the optimal transformation using the correspondences. Compared to the methods that follow the iterative trial-and-error framework, our method establishes correspondences and computes the transformation only once.

### A. Stem Mapping

Existing stem mapping solutions mainly fall into two categories: range image-based methods [30]–[32] and unordered point-based methods [19]–[25]. The former category of methods, taking advantage of the ordered image structure, can efficiently extract tree stems by grouping the pixels of the range image based on local properties. However, range images are not always available, which hampers their use. The latter category of methods slices the point cloud vertically and identifies tree stems by fitting 2D circles or 3D cylinders. A series of contiguous circles or cylinders are then connected to form a complete tree stem. Typically, complex shape fitting (e.g., ellipse [25] or tapered cylinder [21]), skeleton optimization [19], individual tree segmentation [17], [23], supervised point classification [24], and growth direction constraints [22], [25] are used to improve detection integrity and mapping accuracy. However, these computationally intensive steps harm the efficiency of stem mapping. In this work, we introduce a fast stem mapping method to locate stems from raw scans. As our registration method does not require accurate tree attributes, our stem mapping does not have computationally expensive steps for complete stem structure recovery.

### B. Stem-based Registration

Marker-free forest registration techniques generally use tree stems as basic primitives. They broadly fall into two registration frameworks: iterative trial-and-error and inlier-grouping.

1) *Iterative trial-and-error based methods.* In these methods [7]–[16], [18], [26], [27], finding the optimal transformation is achieved through an iterative process. First, a Minimum Sample Set (MSS) is chosen to calculate a transformation. Using this transformation, source stems are then transformed to the coordinate system of target stems. Finally, correspondences are extracted by matching close trees with similar

tree attributes and employed to re-estimate the transformation. The above three steps are iteratively conducted until the optimal transformation (i.e., the one with the largest number of corresponding trees) is found.

These methods are robust but computationally expensive since all the stem positions have to be transformed in each iteration, and thus attempting all possible MSS is not computationally affordable. For example, restricted by the heavy computational burden of examining all possible stem matches, Liang and Hyyppä [9] only manage to achieve 2D horizontal alignment of forest TLS scans and remain the vertical translation unsolved. To enable the practical registration of point clouds of large forest environments, current studies have proposed three strategies to address the computational inefficiency.

The first strategy is to discard unlikely MSS. Specifically, the similarities derived from relative stem positions [10]–[13], [18] and additional tree attributes (e.g., DBH [10]–[13], [18] and tree height [10], [18]) are used to eliminate false MSS and sort the remaining ones. These methods work well for forests of small or medium sizes. However, they remain inefficient when dealing with large-scale forests. For example, the memory usage and execution time of Kelbe et al. [11] can reach prohibitively large when the forest scene has more than 50 trees, while its multi-threaded improved version [13] also takes more than an hour for registering scans containing more than 100 trees. Moreover, these methods can become impractical in plantation forests due to the ambiguities of tree attributes.

The second strategy is to reduce the number of keypoints. Recent studies introduce novel keypoints, e.g., visual occlusion points identified from shaded areas [27] or mode points extracted from tree crowns [14], [26]. Compared to stems, these local keypoints typically have a smaller number. They are used to register forest scans [26], [27] or to guide the stem matching [14] to bypass the computational burden of matching numerous stems. Notwithstanding the enhanced efficiency, these local keypoints require high-quality input point clouds that are still challenging to acquire for complex forest environments [15]. Furthermore, similar to stem positions, the increase of the number of keypoints also results in a dramatic increase in computation time [27].

The third strategy is to use advanced optimization techniques. Ge et al. [15] register multiview forest point clouds by adopting the 4-points congruent sets algorithm [33], [34] that reduces the number of trials required to establish a reliable registration. Polewski et al. [16] apply simulated annealing metaheuristic [35] to determine the optimal corresponding trees between multiplatform LiDAR point clouds. Dai et al. [26] consider the alignment as a maximum likelihood estimation problem and employ the coherent point drift algorithm [36] to fuse forest airborne and terrestrial point clouds.

2) *Inlier-grouping based methods*. This category of methods seeks the optimal transformation in a one-shot manner. Specifically, all corresponding trees (i.e., inliers) are first extracted and then employed to determine the optimal transformation. On the one hand, rather than verifying the transformation and refining correspondences in each iteration as in the iterative

trial-and-error framework, inlier-grouping methods extract correspondences and estimate the transformation only once and are thus generally more efficient [37]. On the other hand, as the transformation is estimated only once, the resulting transformation may not be accurate if the correspondences are unreliable [26], [38]. Therefore, the key of these methods is to extract true correspondences (i.e., inliers) and eliminate false ones (i.e., outliers) [4].

Though the inlier-grouping framework has been widely adopted in registration techniques targeting man-made objects [39]–[41] or urban scenes [4], [42], it is rarely used in forest point cloud registration. To the best of our knowledge, the co-registration approach for multiplatform forest LiDAR data proposed by Guan et al. [17] is the only one that falls into this framework. For each stem position extracted from raw scans via individual tree segmentation, the horizontal coordinates and neighboring stem positions are used to construct a 2D Triangulated Irregular Network (TIN). Then, stem correspondences are extracted by matching 2D TINs (where the matching quality is measured by the number of similar triangles within the TINs) and employed to determine the registration transformation. Their method can reach a satisfactory accuracy (i.e., less than 20 cm) in co-registering multiplatform LiDAR scans, while their running time has not been reported.

In this work, we propose a stem matching method that follows the inlier-grouping framework. We generalize the urban matching approach of Yang et al. [42] to forest environments, and we tailor three main improvements for robust and efficient forest point cloud registration. First, we utilize only geometric coordinates because the semantic features defined in their method are not available in forest environments. Second, by constructing local triangles that encode relative stem positions, we reduce the algorithmic complexity concerning the number of trees from cubic to linear. Last, unlike their greedy grouping algorithm that directly adopts the line-to-line geometric consistency of Chen and Bhanu [39], we propose a graph-to-graph consistency measure that guarantees the robustness in triangle-based correspondence grouping.

### C. Benchmark Datasets

Existing benchmark datasets for point cloud registration typically target man-made objects, indoor scenes, or urban environments [6], [29], [43]–[45]. Very few datasets are publicly available for the evaluation of registration methods for forest point clouds. To the best of our knowledge, WHU-FGI [29] and ETH-Trees [44] are the only two datasets for this purpose, which contain only five and six scans of a single forest plot, respectively. The other FGI forest dataset [46] is intended for assessing tree attribute extraction algorithms, which cannot be used for evaluating registration methods due to the inaccessibility of the registration ground truth. In this work, we release Tongji-Trees, a new benchmark dataset consisting of twenty scans for the comprehensive evaluation of marker-free registration methods for TLS scans of forest areas.

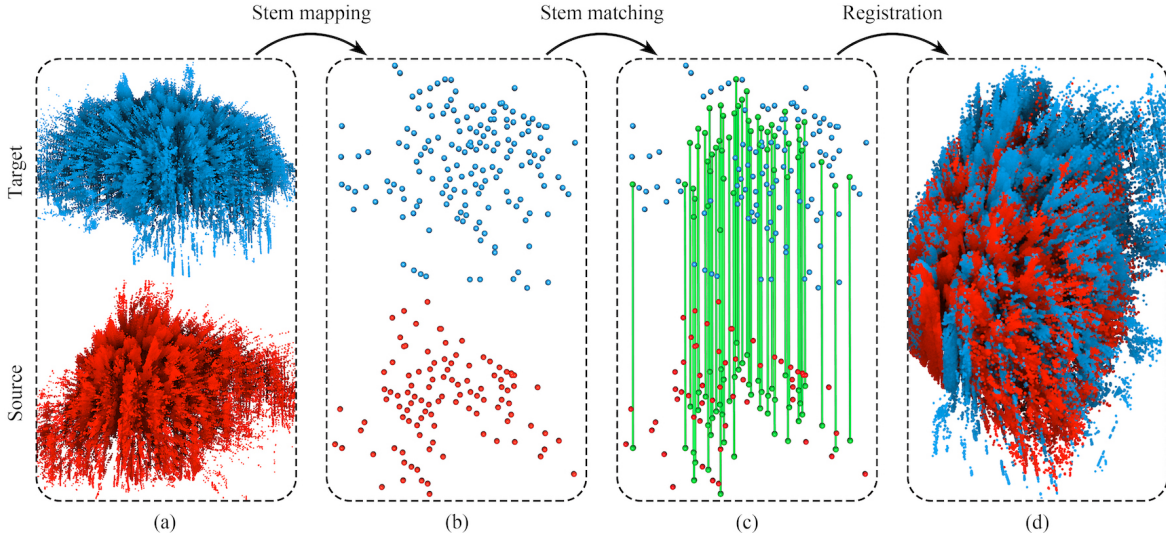


Fig. 2. The pipeline of the proposed method. (a) Input point clouds. (b) Stem positions. (c) Stem matches. (d) Registration result. Given a pair of forest TLS point clouds as input (a), the stem positions of trees are first extracted from each point cloud (b). Then, correspondences between stem positions are established by exploiting relative distances of the stem positions (c). Finally, registration is achieved by applying the transformation computed from the stem correspondences (d).

### III. METHODOLOGY

Our method takes as input a pair of forest TLS scans and outputs a rigid transformation to register the two scans. It consists of three main stages illustrated in Fig. 2: stem mapping, stem matching, and registration, which are detailed as follows.

#### A. Stem Mapping

This stage aims to identify stem positions, i.e., the intersections of stem axes and the ground surface, from a raw TLS scan. This is achieved by first extracting stems, followed by intersecting the stem axes and the ground surface.

To avoid interference from unstable structures such as forest canopy and understory vegetation, we identify the stem points of trees before the extraction of individual stems. To filter out forest canopies, we create a digital terrain model (DTM) based on the input point cloud [47] and mark the points within 0.2–3 m from the DTM as the understory layer. Before excluding understory shrubs, we downsample the data of the understory layer based on a voxel grid with a resolution of 1 cm for efficiency reasons. Considering that tree stems typically have a vertical orientation, we identify tree stems by looking into the pointwise verticality [48], [49] defined as

$$v = 1 - |n_z|, \quad (1)$$

where  $n_z$  represents the third component of the normal vector of a point. A value of 1 indicates that the local surface of a point is perfectly vertically oriented, while a zero value indicates a perfectly horizontal local geometry. In this work, we use a fixed radius of 10 cm for querying the neighbors of a point using the method described in Behley et al. [50] to estimate its normal using principal component analysis [51]. We mark the points whose verticality is higher than a threshold  $\gamma$  as stem points. In all our experiments, we empirically set  $\gamma$  to 0.9. By extracting the stem points, we also significantly

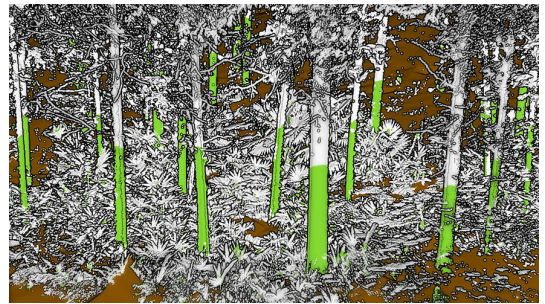


Fig. 3. An example of stem extraction results (a close-up view). The reconstructed DTM is visualized in brown and the extracted tree stems are in green. In this point cloud, the number of points is 30,574,461, while the number of extracted tree stems is only 116. Our method uses the extracted tree stems for registration.

reduce the amount of data to be further processed. Fig. 3 shows an example of the stem extraction results, in which the number of points in the extracted stems is only about 1/80 the size of the initial input.

With the stem points identified from the previous step, we extract individual tree stems by detecting cylinders using the random sample consensus (RANSAC) algorithm [52]. Since detecting multiple cylinders by sequentially applying RANSAC is inefficient and sub-optimal (e.g., a previous wrong detection usually harms the subsequent detection) [53], we first employ the Euclidean clustering algorithm [54] to separate the stem points into small groups each containing a single stem (or in very rare cases few adjacent stems for trees with multi-branch structures near the ground surface). Then for the points of each stem, we apply RANSAC to detect a cylinder. It is worth noting that a few incorrectly detected stems will not affect the subsequent registration because they do not have correspondences in the other point cloud and are thus filtered out in the stem matching stage. Finally, we obtain

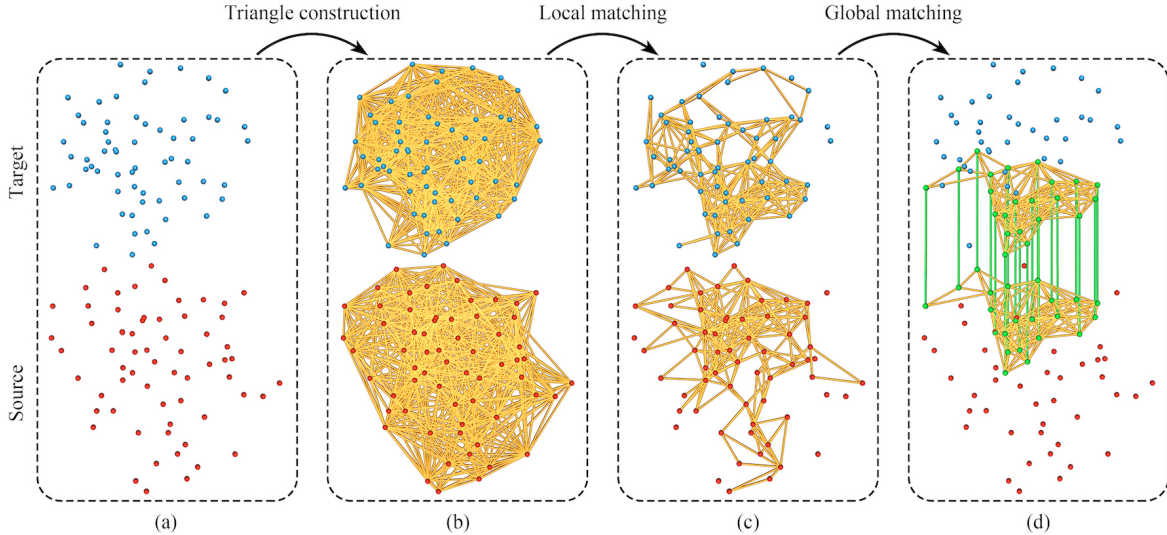


Fig. 4. Stem matching. (a) Stem positions. (b) Triangles encoding the local relative relationship of stem positions. (c) Locally matched triangle pairs. (d) Globally matched triangle pairs and stem matches. In this example, 22 stem matches (denoted by the green lines in (d)) are extracted from 61 target stem positions (denoted by the blue dots in (a)) and 64 source stem positions (denoted by the red dots in (a)). The numbers of initial triangles for the target and source scans are respectively 1725 and 1789 (b). The numbers of locally and globally matched triangle pairs are 210 (c) and 154 (d), respectively.

a set of stem positions  $\mathcal{L} = \{1_i, 1 \leq i \leq N_i\}$  by intersecting the axes of the cylinders with the DTM model, where  $N_i$  denotes the number of stem positions.

### B. Stem Matching

The goal of this stage is to establish the correspondences between the previously extracted stem positions of the two input point clouds. Our stem matching method differs from the existing methods in the following two aspects: (1) it requires only the information of stem positions while existing methods also require additional tree attributes, such as DBH, tree height, or tree crown [10]–[15], [18]; (2) our stem matching is a deterministic non-iterative process while existing methods [7]–[16], [18], [26], [27] follow an iterative trial-and-error procedure that is less efficient.

Our stem matching consists of three steps as shown in Fig. 4. We first construct a set of local triangles for each scan from its stem positions to encode their relative spatial relationship. These triangles are then matched in the subsequent local matching and global matching steps to obtain the correspondences between the stem positions of the two input scans. In the following, we elaborate on each step of our stem matching algorithm.

1) *Triangle construction.* Previous studies [11]–[14] commonly use an exhaustive approach to create triangles from the stem positions, i.e., any triplet of stem positions forms a triangle. Thus, the number of triangle pairs to be verified using this exhaustive approach is

$$\binom{M}{3} \cdot \binom{N}{3}, \quad (2)$$

where  $M$  and  $N$  denote the number of stems in the source and target scans, respectively. With this exhaustive approach, the number of triangles to be matched increases explosively with the number of stems extracted from the input point clouds.

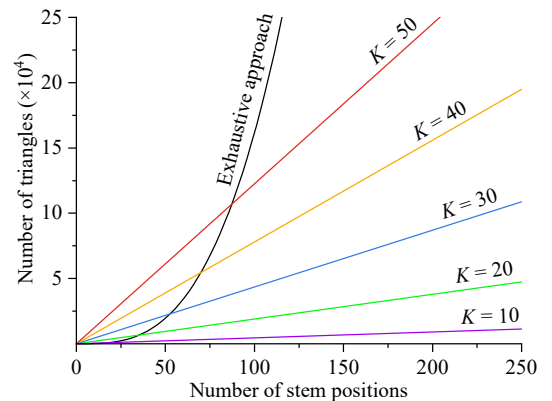


Fig. 5. The number of triangles to be matched with respect to neighborhood size (i.e., the  $K$  value).

We observe that only certain triangles whose vertices have correspondences in the other point cloud contribute to stem matching and it is sufficient to build triangles by only connecting the adjacent stem positions. To this end, we construct only local triangles by connecting every stem position with its  $K$ -nearest stem positions. This simple strategy significantly reduces the complexity of triangle matching from  $\mathcal{O}(M^3 \cdot N^3)$  to  $\mathcal{O}(M \cdot N)$ . Specifically, for a scan containing  $N_i$  detected stem positions, the number of triangles to be matched increases linearly instead of cubically with the number of stem positions, i.e.,

$$\mathcal{O}\left(\frac{1}{6}N_i^3 - \frac{1}{2}N_i^2 + \frac{1}{3}N_i\right) \rightarrow \mathcal{O}\left(\frac{K^2 - K}{2}N_i\right). \quad (3)$$

Fig. 5 depicts how the number of triangles increases concerning different  $K$  values, and that of the exhaustive approach. In our implementation, we set  $K$  to 20, which ensures sufficient local triangles to be constructed to establish the correspondences between the two sets of stem positions.

With the set of triangles  $\mathcal{T}^* = \{t_i^*, 1 \leq i \leq N_t^*\}$  constructed from the source scan and the set of triangles  $\mathcal{T}' = \{t'_i, 1 \leq i \leq N_t'\}$  constructed from the target scan, where  $N_t^*$  and  $N_t'$  denote the numbers of triangles in the source and target scans respectively, we establish the correspondences between the source and target triangles in two steps: a local matching step and a global matching step.

2) *Local matching*. In this step, we establish triangle-wise correspondences between the two sets of triangles. This can be easily achieved by comparing the edge lengths of two triangles from the two sets. For efficiency reasons, we first sort the vertices of each triangle such that the one opposite to the longest edge comes first and the triangle is in counter-clockwise orientation. The following lemma lays the foundation for our triangle-wise local matching.

**Lemma 1.** *If three stem positions in the source scan  $l_i^*, l_j^*, l_k^* \in \mathcal{L}^*$  have correspondences in the target scan  $l'_i, l'_j, l'_k \in \mathcal{L}'$ , the source triangle  $\Delta l_i^* l_j^* l_k^* \in \mathcal{T}^*$  is congruent with the target triangle  $\Delta l'_i l'_j l'_k \in \mathcal{T}'$ .*

As the contrapositive of Lemma 1, the following lemma is equally true:

**Lemma 2.** *Given three pairs of stem positions  $\langle l_i^*, l'_i \rangle$ ,  $\langle l_j^*, l'_j \rangle$ ,  $\langle l_k^*, l'_k \rangle$ , if the source triangle  $\Delta l_i^* l_j^* l_k^* \in \mathcal{T}^*$  is not congruent with the target triangle  $\Delta l'_i l'_j l'_k \in \mathcal{T}'$ , then at least one pair of the stem positions does not match.*

By verifying any pair of source and target triangles, we accumulate potentially matched triangle pairs (Lemma 1) and filter out false matches (Lemma 2). In our work, we define the local dissimilarity between two triangles  $t_1$  and  $t_2$  as

$$D_{local}(t_1, t_2) = \sum_{i=1}^3 |\varepsilon_i^* - \varepsilon'_i|, \forall |\varepsilon_i^* - \varepsilon'_i| < \epsilon, \quad (4)$$

where  $\varepsilon_i^*$  and  $\varepsilon'_i$  denote the length of the corresponding edges in the two triangles.  $\epsilon$  is the maximum allowed difference in edge length for two triangles to be matched, which is empirically set to 5 cm in all our experiments. Note that if the difference in edge length of any pair of edges is greater than  $\epsilon$ , the two triangles are not considered matched. For each triangle  $t'_j$  in the target scan, we find its potential corresponding triangle  $t_i^*$  in the source scan as the one that has the minimum dissimilarity value, resulting in a locally matched triangle pair  $u = \langle t_i^*, t'_j \rangle$ .

After local matching, a considerable portion of triangles for which local matches could not be found will be deleted. It should be noted that two triangles being congruent is only a necessary condition for the stem positions (encoded in their vertices) to be correspondent, but it is not sufficient.

3) *Global matching*. This step aims to establish the correspondences between the two sets of stem positions encoded in the source triangles and target triangles respectively. In theory, this can be achieved by matching two undirected fully connected graphs whose vertices are the stem positions of the source and target scans, respectively. We approach the graph matching by looking for the largest consensus set of the two graphs.

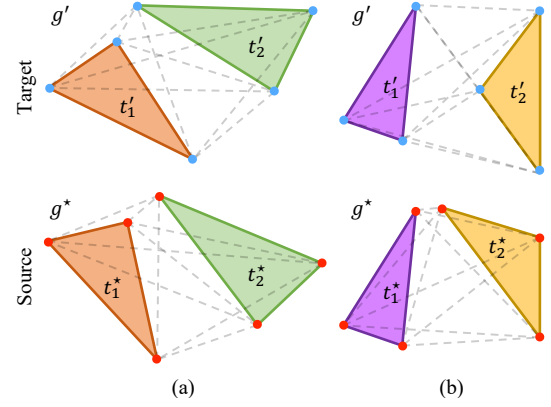


Fig. 6. Two examples illustrating the global dissimilarity between two locally matched triangle pairs  $u_1 = \langle t_1^*, t_1' \rangle$  and  $u_2 = \langle t_2^*, t_2' \rangle$ . (a)  $u_1$  and  $u_2$  form a consensus set, i.e.,  $D_{global}(u_1, u_2) < \epsilon$ . (b)  $u_2$  does not agree with  $u_1$  (i.e.,  $D_{global}(u_1, u_2) > \epsilon$ ) and thus they cannot form a consensus set.

Unlike the local matching step that compares individual triangles, our global matching step uses triangle pairs as primitives. Before explaining our global matching, we first define a metric called global dissimilarity to measure the consistency between two pairs of locally matched triangles. Given two locally matched triangle pairs  $u_1 = \langle t_1^*, t_1' \rangle$  and  $u_2 = \langle t_2^*, t_2' \rangle$  (see Fig. 6), we build two undirected fully connected graphs, i.e.,  $g^*$  from the vertices of  $t_1^*$  and  $t_2^*$ , and  $g'$  from the vertices of  $t_1'$  and  $t_2'$ . Then the global dissimilarity between the two locally matched triangle pairs  $u_1$  and  $u_2$  is defined as

$$D_{global}(u_1, u_2) = \max |\mathcal{E}_i^* - \mathcal{E}'_i|, \quad (5)$$

where  $\mathcal{E}_i^*$  and  $\mathcal{E}'_i$  denote the lengths of the corresponding edges respectively in  $g^*$  and  $g'$ . Since  $t_1^*$  and  $t_1'$ ,  $t_2^*$  and  $t_2'$  are respective congruent triangle pairs, it is sufficient to test only the edges connecting vertices of different triangles (i.e., the edges denoted by the dashed lines in Fig. 6).  $D_{global}$  measures how much adding a new pair of locally matched triangles disagrees with an existing pair. If a locally matched triangle pair is consistent with any existing pair, we call it a globally matched pair, just to differentiate it from the locally matched pairs. Note that Yang et al. [42] compare only the relative positions of the centroids of two triangles, which has ambiguities. See Fig. 6(b) for an example, where the distance between the centroids of  $t_1^*$  and  $t_2^*$  is identical to that of  $t_1'$  and  $t_2'$  but the two pairs of triangles do not match.

We obtain the optimal correspondences between the two sets of stem positions by finding the largest consensus set. For each locally matched triangle pair  $u_i$ , our method grows a consensus set by accumulating globally matched triangle pairs  $u_j$  that agrees with  $u_i$  (i.e.,  $D_{global}(u_i, u_j) < \epsilon$ , where  $\epsilon$  is the same threshold used in the local matching step). Fig. 7 illustrates the growth of a consensus set of globally matched triangle pairs. Each consensus set grows independently and the one that has accumulated the most globally matched triangle pairs gives us the optimal correspondences between the two sets of stem positions. The process for finding the largest consensus set is detailed in Algorithm 1.

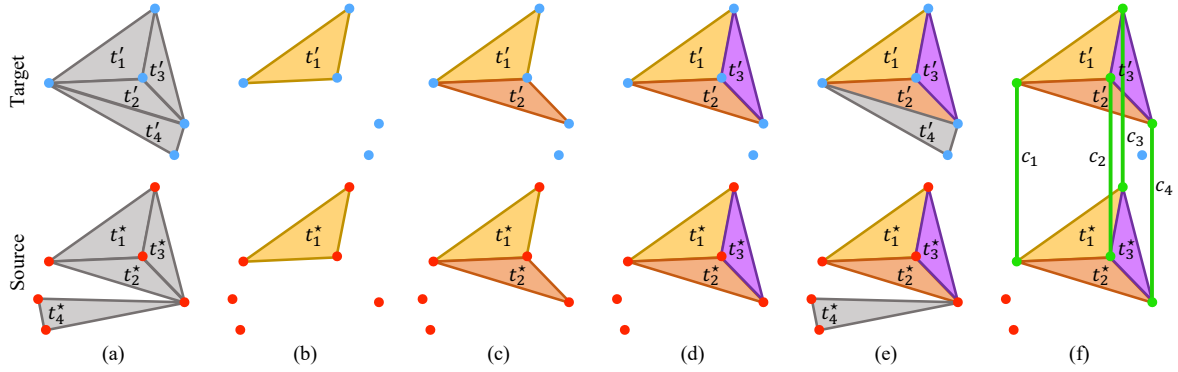


Fig. 7. An example illustrating the growth of a consensus set. Given an initial set of locally matched triangle pairs  $\mathcal{U} = \{u_1, u_2, u_3, u_4\}$ ,  $u_i = \langle t_i^*, t_i' \rangle$  (a), our algorithm starts accumulating globally matched triangle pairs from an initial pair  $\langle t_1^*, t_1' \rangle$  (b). In each iteration, our method tries to find one more globally matched triangle pair and adds it to the growing set (c) and (d). The growing process stops when no more triangle pair that is consistent with the initial pair can be found. In this example, the triangle pair  $u_4$  does not agree with the initial pair  $u_1$  due to  $D_{global}(u_1, u_4) > \epsilon$  (e). Finally, a set of globally matched triangle pairs  $\mathcal{U}^\dagger = \{u_1, u_2, u_3\}$  is obtained, giving us the correspondences of the stem positions  $\mathcal{C} = \{c_1, c_2, c_3, c_4\}$  (f). The correspondences are denoted by the green lines connecting the stem positions of the two scans.

It is worth noting that the growth of a consensus set can be immediately stopped when a sufficient number of globally matched triangle pairs have been accumulated. However, the growing process only involves comparing edge lengths and it is quite efficient to find the largest consensus set using an exhaustive search because of the small number of triangle pairs that remained after the local matching step. Such an exhaustive search guarantees the optimal consensus set is always used for the registration, ensuring robustness in registration. Note that our exhaustive search in the global matching step is carried out over the already matched local triangle pairs, which differs fundamentally from existing methods where the exhaustive search is performed on the two entire sets of stem positions. The computational complexity of our global matching is several orders of magnitude smaller than that of existing methods.

### C. Registration

From the correspondences of stem positions, a rigid transformation can be computed to register the two input scans. This transformation has 6 Degrees-of-Freedom (DoFs) and can be written as a  $4 \times 4$  matrix with the following structure

$$\mathbf{T} = \begin{bmatrix} \mathbf{R} & \mathbf{t} \\ \mathbf{0} & 1 \end{bmatrix} = \begin{bmatrix} R_{11} & R_{12} & R_{13} & t_x \\ R_{21} & R_{22} & R_{23} & t_y \\ R_{31} & R_{32} & R_{33} & t_z \\ 0 & 0 & 0 & 1 \end{bmatrix}, \quad (6)$$

where  $\mathbf{R}$  is the 3-DoF rotation and  $\mathbf{t}$  is the 3-DoF translation. More information about computing a rigid transformation from a set of correspondences can be found in Sorkine-Hornung and Rabinovich [55].

Using the above computed transformation, we can register the two input point clouds into the same coordinate system. Considering that scanners nowadays typically produce well-leveled point clouds (i.e., the Z axis of the point cloud points upward), the complexity of the registration problem for such data can be reduced to 4-DoF, i.e., a translation (3 DoFs) and

---

### Algorithm 1 Global matching

---

**Input:** a set of locally matched triangle pairs  $\mathcal{U}$

**Output:** correspondences of stem positions  $\mathcal{C}$

- 1: **Initialization:**  $\mathcal{C} \leftarrow \emptyset$ ; each consensus set  $\mathcal{U}_i^\dagger \leftarrow \emptyset$
  - 2: **for** each  $u_i \in \mathcal{U}$  **do**
  - 3:   insert  $u_i$  into  $\mathcal{U}_i^\dagger$
  - 4:   **for** each  $u_j \in \mathcal{U}, i \neq j$  **do**
  - 5:     **if**  $D_{global}(u_i, u_j) < \epsilon$  **then**
  - 6:       insert  $u_j$  into  $\mathcal{U}_i^\dagger$
  - 7:     **end if**
  - 8:   **end for**
  - 9: **end for**
  - 10:  $\mathcal{U}_{max}^\dagger \leftarrow \max(\{\mathcal{U}_i^\dagger\})$
  - 11: **for** each pair of corresponding vertices  $c_i \in \mathcal{U}_{max}^\dagger$  **do**
  - 12:   insert  $c_i$  into  $\mathcal{C}$
  - 13: **end for**
- 

a rotation around the Z axis (1 DoF), and the final registration transformation has the following structure,

$$\hat{\mathbf{T}} = \begin{bmatrix} \mathbf{R}(\phi) & \mathbf{t} \\ \mathbf{0} & 1 \end{bmatrix} = \begin{bmatrix} \cos \phi & -\sin \phi & 0 & t_x \\ \sin \phi & \cos \phi & 0 & t_y \\ 0 & 0 & 1 & t_z \\ 0 & 0 & 0 & 1 \end{bmatrix}, \quad (7)$$

where  $\mathbf{R}(\phi)$  defines the 1-DoF rotation about the azimuth  $\phi$ . In this case, the 4-DoF registration can be achieved by the alignment of the two scans in the 2D horizontal direction (3 DoFs) and an 1D vertical translation (1 DoF). Specifically, with the  $x$  and  $y$  coordinates of the corresponding stem positions, we estimate the 2D horizontal registration parameters  $\phi$ ,  $t_x$ , and  $t_y$  by solving a least-squares problem [55]. Using the  $z$  coordinates of the corresponding stem positions  $\langle z_i^*, z_i' \rangle$ , we calculate the vertical translation  $t_z = \frac{1}{N_c} \sum_{i=1}^{N_c} (z_i' - z_i^*)$ , where  $N_c$  is the number of correspondences of stem positions.

Our method allows both 6-DoF registration and 4-DoF registration. When aligning forest TLS scans that are well leveled, the 4-DoF solution is preferred since it takes advantage of the scanners and may achieve better coarse registration

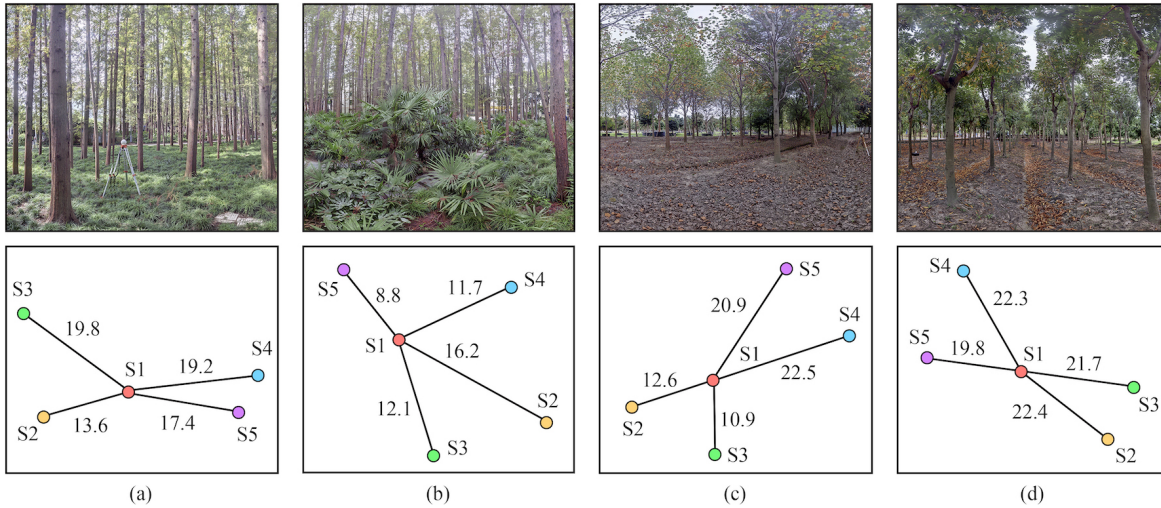


Fig. 8. The four plots of the Tongji-Trees dataset. (a) Plot #1. (b) Plot #2. (c) Plot #3. (d) Plot #4. The top row shows a representative view and the bottom row shows the five scanning positions (S1–S5) for each plot. The numbers indicate the distances (in meters) between the related scanning positions.

TABLE I  
STATISTICS ON THE TONGJI-TREES BENCHMARK DATASET

Plot ID	Main tree species	Plot size (m <sup>2</sup> )	Tree height (m)	Tree density (trees/ha)	Number of points of each scan				
					S1	S2	S3	S4	S5
#1	Metasequoia	65 × 50	19	1036	33,540,068	33,469,682	13,553,220	34,488,581	33,652,969
#2	Metasequoia	90 × 50	23	1210	33,661,875	33,891,812	30,574,461	34,193,448	33,197,039
#3	Liriodendron chinense	80 × 40	7	433	35,510,140	35,169,411	33,680,749	33,445,603	37,076,208
#4	Sapindus mukorossi	65 × 55	10	982	37,189,070	35,274,954	37,113,902	35,598,180	35,783,768

accuracy (see Section V-D). After the coarse registration of the two scans, we further improve the registration using the iterative closest points (ICP) algorithm [56].

#### IV. BENCHMARK DATASET

##### A. Study Areas

The Tongji-Trees dataset contains TLS scans of four plantation forest plots, which were collected in Shanghai, China (31.15°N, 121.12°E). The plot size varies from Plots #1 to #4, with a cover area of 65 × 50, 90 × 50, 80 × 40, and 65 × 55 m<sup>2</sup>, respectively. Metasequoia trees are irregularly distributed in Plots #1 and #2, with an average height of 19 m and 23 m and a density of 1036 trees/ha and 1210 trees/ha, respectively. As for Plots #3 and #4, Liriodendron chinense trees with an average height of 7 m and Sapindus mukorossi trees with an average height of 10 m were planted in rows with spacing of 5 m and 3 m, respectively. Compared to Plots #1 and #2, Plots #3 and #4 are sparser, with a density of 433 trees/ha and 982 trees/ha, respectively. As shown in the top row of Fig. 8, the surface of Plot #1 is covered with wild grass. Plot #2 is partially overgrown with breast-high shrubs. Both Plots #3 and #4 have bare but humped surfaces. The mutual occlusion of complex shrubs in Plot #2 makes it more challenging for registration than the other plots. Table I summarizes the information of all the plots in the Tongji-Trees dataset.

##### B. Data Acquisition

By exploiting the “multi-scan” data acquisition approach [3], each of the four plots was scanned at five positions,

i.e., one at the center and the other four away around the center, forming five scans for each plot and twenty scans for the whole dataset. The bottom row of Fig. 8 illustrates the scanner positions for each plot in the Tongji-Trees dataset. During field surveys, we used a Z+F 5010C terrestrial laser scanner to capture the point cloud data. The scanner has a measurement accuracy of ±3 mm at 50 m, a measurement range of 0.3–180 m, and a view angle of 360° × 320°.

##### C. Ground Truth

Before scanning, we strictly leveled the scanner and set up spherical reference markers that could help us to produce correspondences for deriving the ground-truth registration transformation. Each marker was mounted on a tripod or placed stably on the ground (rather than fixed on tree stems, which usually causes occlusions). Each raw scan contains about 30-million points (see Table I), with each point represented as a 7D vector ( $xyz$  coordinates,  $rgb$  colors, and an intensity value). Although our registration method relies on 3D coordinates only, the provided attributes may benefit other methods or studies. We identified the markers and served them as correspondences to compute the ground-truth transformation matrix for every possible pair of scans. The ground-truth transformation matrices can be used to evaluate the performance of registration methods.



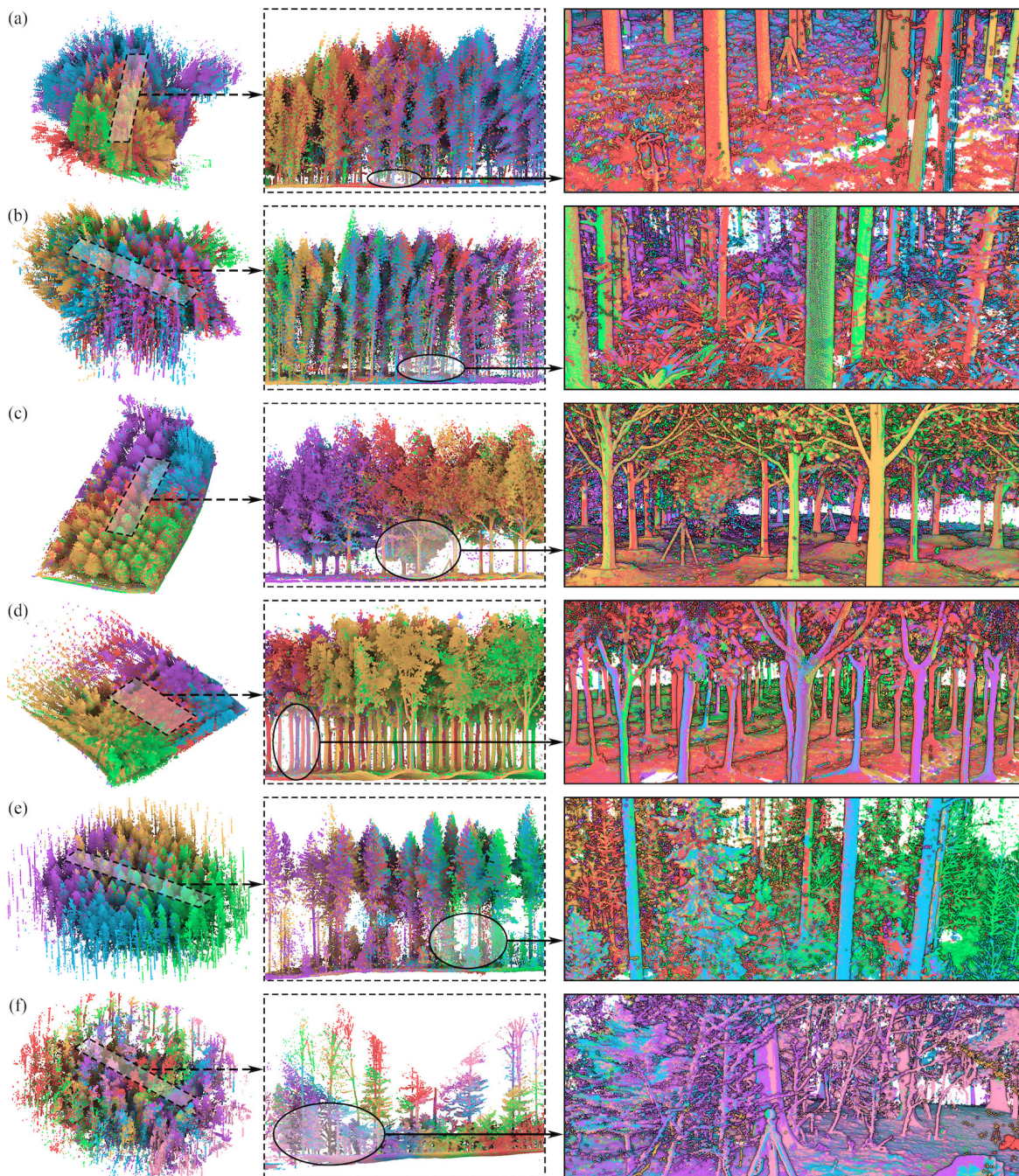


Fig. 9. Registration results on the three test datasets. (a) to (d) Plots #1–#4 of the Tongji-Trees dataset, respectively. (e) WHU-FGI [29]. (f) ETH-Trees [44]. From left to right: an overview, a cross-section, and a close-up view of the registered point clouds of each plot. Scans S1–S5 in each plot are visualized in red, yellow, green, blue, and purple colors, respectively, and the S6 of ETH-Trees is in pink.

## V. RESULTS AND DISCUSSION

### A. Implementation Details

We have implemented our algorithm using C++ based on the Point Cloud Library [57]. For efficiency, we parallelized computationally intensive parts of the proposed algorithm using OpenMP [58]. Specifically, the following parts of our algorithm are parallelized:

- neighborhood query, verticality calculation, cylinder detection, and stem position computation in the stem mapping stage;

- local matching and global matching in the stem matching stage.

All experiments were carried out on a laptop with an Intel Core 2.60 GHz i7 CPU (8 threads) and 32 GB RAM.

### B. Test Datasets and Evaluation Metrics

We have tested the proposed method on our Tongji-Trees dataset, the WHU-FGI dataset [29], and the ETH-Trees dataset [44]. The WHU-FGI dataset contains five scans captured from a  $32 \times 32$  m<sup>2</sup> plot of a natural forest dominated

by Scots pines, located at Evo, Finland (61.19°N, 25.11°E). The ETH-Trees dataset consists of six scans acquired in a forest with a large amount of underwood.

To quantitatively evaluate the performance of registration methods, we have recorded both the matrix-based errors and point-wise errors.

- Matrix-based errors, i.e., the rotation error  $e_R$  and the translation error  $e_t$  between the estimated transformation parameters  $\mathbf{R}$ ,  $\mathbf{t}$  and the corresponding ground-truth values  $\tilde{\mathbf{R}}$ ,  $\tilde{\mathbf{t}}$ :

$$e_R = \arccos\left(\frac{\text{tr}(\tilde{\mathbf{R}}\mathbf{R}^T) - 1}{2}\right) \frac{180}{\pi}, \quad (8)$$

$$e_t = \|\tilde{\mathbf{t}} - \mathbf{t}\|, \quad (9)$$

where  $e_R$  measures the difference between the two rotation matrices  $\mathbf{R}$  and  $\tilde{\mathbf{R}}$ , and  $e_t$  quantifies the magnitude of the difference of the two translation vectors  $\mathbf{t}$  and  $\tilde{\mathbf{t}}$ . It is worth noting that a better registration method may not outperform other methods in terms of both rotation error and translation error.

- Pointwise error, proposed by Chen et al. [6]. Given a source scan  $\mathcal{P}^* = \{\mathbf{p}_i^*, 1 \leq i \leq N_p^*\}$  containing  $N_p^*$  points, the pointwise error is defined as

$$e_p = \frac{1}{N_p^*} \sum_{i=1}^{N_p^*} \left\| \mathbf{R}\mathbf{p}_i^* + \mathbf{t} - (\tilde{\mathbf{R}}\mathbf{p}_i^* + \tilde{\mathbf{t}}) \right\|. \quad (10)$$

Compared to the matrix-based errors, the pointwise error is more intuitive in comparing the performance of different registration methods.

### C. Registration Results

Following the previous works, e.g., [9], [10], [13], [14], [27], we aligned scans at the corners of each plot to the one at the center. This is a common practice for registering point clouds of LiDAR-based forest inventory.

Fig. 9 demonstrates the final registration results of our proposed method on the three test datasets. As can be seen from the close-up view of the registration result of each plot, our method properly registered all TLS scans from diverse forest environments. The test datasets contain both sparse forests (with a tree density below 500 trees/ha, as shown in Fig. 9(c) and (e)) and dense forests (with a tree density around 1000 trees/ha, as shown in Fig. 9(a), (b), and (d)).

TABLE II  
FINE REGISTRATION ERRORS OF THE PROPOSED METHOD

Plot ID	Forest environment		Fine registration errors		
	Tree locations	Understory	$e_p$ (cm)	$e_R$ (°)	$e_t$ (cm)
Plot #1	Dense, scattered	Wild grass	0.7	1.9	0.7
Plot #2	Dense, scattered	High shrub	1.3	4.1	1.0
Plot #3	Sparse, regular	Bare ground	0.9	1.2	0.8
Plot #4	Dense, regular	Bare ground	1.0	1.2	1.0
WHU-FGI	Sparse, scattered	Underwood	1.6	3.1	1.4
ETH-Trees	Sparse, scattered	Underwood	0.8	3.0	0.6
Average			1.0	2.4	0.9

Since our method has linear complexity to the number of trees, it can register the scans of both sparse and dense forests. Compared to plots covered in wild grass (see Fig. 9(a)) and plots having bare ground (see Fig. 9(c) and (d)), Plot #2 is partially overgrown with breast-high shrubs (see Fig. 9(b)), whereas the WHU-FGI and ETH-Trees datasets contain a large amount of underwood. Despite the complex understory structures, our method still extracted valid stem positions and managed to register these point clouds. Our method is also robust to the distribution of trees. It correctly aligned scans containing scattered trees (Fig. 9(a), (b), (e), and (f)) and scans consisting of trees planted in rows (Fig. 9(c) and (d)). Besides, our registration method succeeded on different tree species, i.e., Metasequoia (Fig. 9(a) and (b)), Liriodendron chinense (Fig. 9(c)), Sapindus mukorossi (Fig. 9(d)), and Scots pines (Fig. 9(e)).

Table II reports a quantitative evaluation of our registration results. The average pointwise error of all test plots is 1 cm, showing the great potential of the proposed approach to substitute the costly marker-based methods.

### D. 6-DoF Registration versus 4-DoF Registration

As has been explained in Section III-C, our method allows both 6-DoF registration and 4-DoF registration for well-leveled TLS forest scans, and for such data, the 4-DoF solution is preferred. To understand the effectiveness of both the 6-DoF registration and the 4-DoF registration strategies, we compared them using the three test datasets. This comparison has revealed that the coarse registration results from both the 6-DoF and the 4-DoF strategies are sufficiently accurate for the subsequent ICP fine registration to converge. We further computed the horizontal and vertical deviations of the pointwise errors and depicted them in a box plot shown in Fig. 10. From this figure, we can see that the 4-DoF registration results are more accurate than those from the 6-DoF registration, and the 4-DoF registration strategy is remarkably accurate in the horizontal direction (with a mean horizontal pointwise error

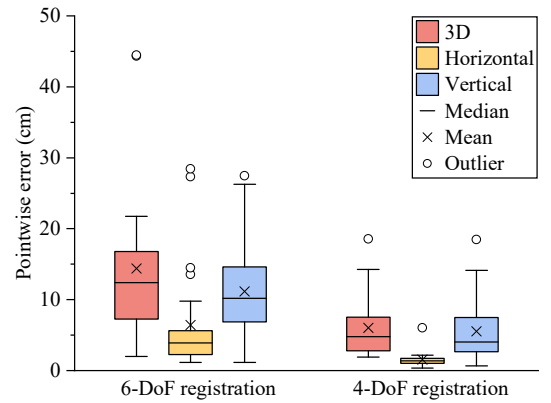


Fig. 10. Box plot showing the horizontal and vertical deviations of pointwise registration errors, for both the 6-DoF registration and the 4-DoF registration. “3D” denotes the pointwise error, while “Horizontal” and “Vertical” represent the horizontal and vertical components of the pointwise error, respectively. “Mean” and “Median” are the respective average and middle values of all pointwise errors. “Outlier” is defined as an error value located outside the whiskers of the box plot.

of only 1.5 cm). The 4-DoF strategy is more accurate because it takes the advantage of the well-leveled scans.

It is also worth noting that the registration errors in the vertical direction are greater than in the horizontal direction. This is a common limitation of the stem-based methods [10], [11], [13]–[15] because stem positions are more accurate in the horizontal direction than those in the vertical direction. In other words, the  $z$  coordinates of the extracted stem positions are more sensitive to the change of DTM, compared with their  $x$  and  $y$  coordinates, as illustrated in Fig. 11(a). The registration results depicted as outliers in Fig. 10 were obtained for the scans in Plot #2 and ETH-Trees where the ground near stems was severely occluded by understory vegetation, leading to large errors in the  $z$  coordinates of the stem positions. This can be explained from the illustration shown in Fig. 11(b). Such a test indicated that by decomposing the registration problem into two sub-problems, i.e., horizontal alignment and vertical alignment, the 4-DoF strategy can take advantage of the accurate horizontal coordinates of stem positions.

### E. Comparison

We have compared our method with three existing coarse registration algorithms: TOA [11], Fast-TOA [13], and FMP+BnB [4]. TOA and Fast-TOA are both tree-oriented approaches and are often used as the baseline methods for evaluating forest point cloud registration methods. Fast-TOA is a multi-threaded variant of TOA. FMP+BnB is a two-step method combining fast match pruning and branch-and-bound, which is one of the state-of-the-art methods for pairwise registration of general TLS scans. Note that TOA and Fast-TOA are not end-to-end solutions: they cannot directly consume raw point clouds but require stem maps (i.e., stem positions and DBHs) as input. For a fair comparison, we prepared stem maps for every scan as has been done in the Fast-TOA paper [13]. Moreover, TOA was not able to produce any results for scans containing a large number (e.g., greater than 70) of trees. Fast-TOA also becomes quite inefficient when handling point clouds consisting of more than 100 trees. For example, it took over an hour to register two scans containing only 117 and 109 trees, respectively. Hence, we had to reduce the number of trees in every stem map to approximately 50 (similar to the number of trees in the experimental data used in the original paper [13]) to be able to conduct the comparison. To guarantee the sufficient overlap between each pair of simplified stem maps, we manually selected these 50 stems to include all corresponding ones.

We have recorded both the matrix-based errors, the pointwise error, and the running time of each method. The registration errors are reported in Table III. Our method outperforms the others in terms of registration accuracy on three of the six test plots and achieves the best overall performance with a minimum average pointwise error of 5.9 cm.

### F. Robustness w.r.t. Overlap Ratio

We have also tried to exhaustively register all scan pairs of each plot to understand the robustness of our method concerning overlap ratio. The three datasets form a total of

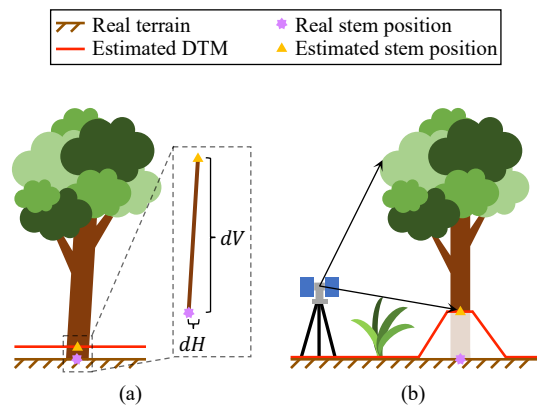


Fig. 11. Inaccuracy in the extracted stem positions. (a) The vertical component of stem positions is sensitive to the change of DTM. (b) Insufficient ground data (due to occlusions) results in a large error in the  $z$  coordinate of the stem position.

TABLE III  
ACCURACY COMPARISON WITH THREE COMPETING ALGORITHMS

Plot ID	Method	Coarse registration errors		
		$e_p$ (cm)	$e_R$ (')	$e_t$ (cm)
Plot #1	TOA	11.0	37.3	8.7
	Fast-TOA	9.4	31.6	6.7
	FMP+BnB	9.1	11.1	8.8
	Ours	<b>6.2</b>	2.6	6.2
Plot #2	TOA	27.8	77.0	21.4
	Fast-TOA	27.3	85.0	19.7
	FMP+BnB	6.6	8.6	6.3
	Ours	<b>6.2</b>	4.2	6.0
Plot #3	TOA	1.4	5.0	1.3
	Fast-TOA	<b>1.3</b>	4.4	1.2
	FMP+BnB	3.5	3.7	3.5
	Ours	3.6	1.7	3.6
Plot #4	TOA	3.9	12.3	3.8
	Fast-TOA	3.7	12.4	3.5
	FMP+BnB	6.3	6.2	6.3
	Ours	<b>3.1</b>	1.0	3.1
WHU-FGI	TOA	7.6	26.0	5.5
	Fast-TOA	<b>6.1</b>	25.8	3.7
	FMP+BnB	7.3	12.2	6.9
	Ours	7.6	2.1	7.6
ETH-Trees	TOA	20.7	78.2	18.2
	Fast-TOA	22.2	68.6	20.0
	FMP+BnB	<b>5.0</b>	12.5	4.5
	Ours	8.7	11.7	8.6
Average	TOA	12.1	39.3	9.8
	Fast-TOA	11.7	38.0	9.1
	FMP+BnB	6.3	9.0	6.1
	Ours	<b>5.9</b>	3.9	5.8

65 scan pairs. Some of these scan pairs have small overlap (see Fig. 13), which usually fails marker-free registration methods. By providing simplified stem maps ( $\sim 50$  trees/scan), TOA registered 59 scan pairs while Fast-TOA succeed on 61. FMP+BnB failed in aligning almost a quarter of scan pairs (with only 48 successful) due to the limited overlap of the input scan pairs. In contrast, our method managed to register all the 65 raw scan pairs. We have recorded the success rate of all competing methods on the coarse registration of each plot. The results are reported in Table IV, from which we can see that the forest-oriented registration methods (i.e.,

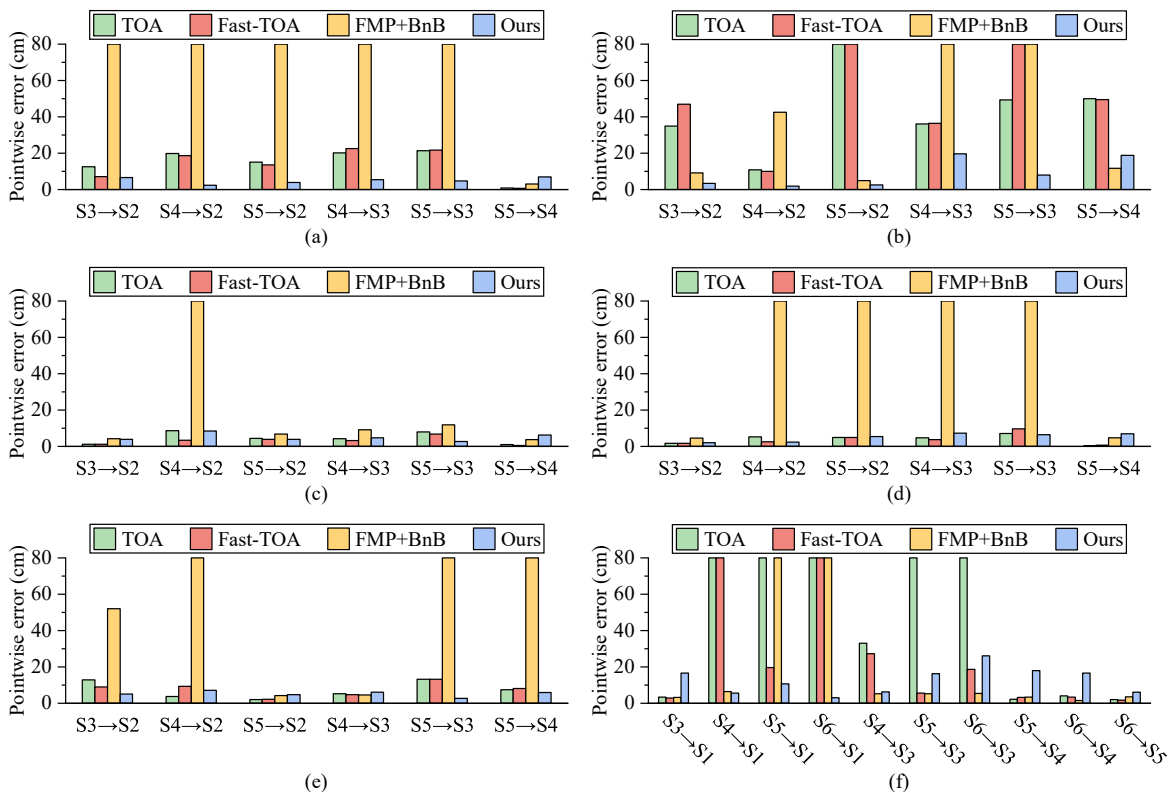


Fig. 12. Pointwise errors for the registration of all other scan pairs in each plot of the three test datasets (in addition to the registration accuracy reported in Table III). (a) to (d) Plots #1–#4 of the Tongji-Trees dataset, respectively. (e) WHU-FGI [29]. (f) ETH-Trees [44]. Note, the pointwise error for any failed registration (i.e., registration with a pointwise error greater than 10 m) is truncated to 80 cm for the visualization purpose.

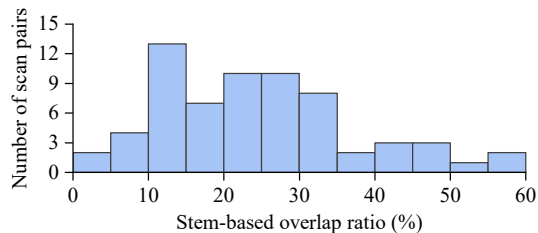


Fig. 13. Histogram of stem-based overlap ratios on all scan pairs of the three test datasets.

TOA, Fast-TOA, and ours) are more robust than the general local descriptor-based methods (i.e., FMP+BnB). Among these methods, our method has the highest successful registration rate (i.e., no failure cases).

In addition to the registration errors reported in Table III, we also recorded the pointwise errors for the registration of all other scan pairs in each plot of the three test datasets. From the results demonstrated in Fig. 12, we can see that our method outperforms the competing methods on most of the scan pairs.

### G. Efficiency

The running times of our method are reported in Fig. 14. The average running times of the stem mapping and stem matching stages are 14.1 seconds and 0.6 seconds, respectively. The stem mapping stage takes most of the time, while the stem matching stage is relatively fast, taking less than three

TABLE IV  
SUCCESS RATES OF ALL COARSE REGISTRATION METHODS

Method	Success rate of coarse registration (%)						
	Plot #1	Plot #2	Plot #3	Plot #4	FGI	ETH	Average
TOA	100	90	100	100	100	67	91
Fast-TOA	100	80	100	100	100	87	94
FMP+BnB	50	80	90	60	70	87	74
Ours	100	100	100	100	100	100	<b>100</b>

seconds even when handling scans containing a large number of trees (more than 200 trees/scan).

Fig. 15 reports the running times of our proposed method and the competing methods. We can see that our approach is much faster than the two stem-based methods, i.e., TOA and Fast-TOA, even their preparation times of stem maps were not counted and their input was already simplified. Notably, TOA (relying heavily on DBH values) took unacceptably long times on Plot #3, Plot #4, and ETH-Trees because trees in these plots have similar attributes. Our method tackles the inefficiency problem of the stem-based strategy by significantly reducing the complexity of stem matching, which allows it to handle scans containing a large number of trees and leads to consistently high efficiency. Compared to the local-descriptor-based approach FMP+BnB that intends to accelerate the coarse registration of general TLS scans, the running time of our method is only 1/6 of it on average.

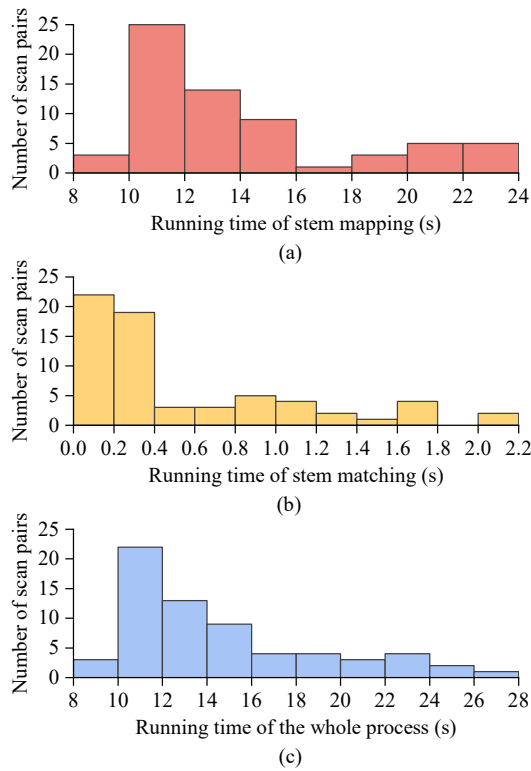


Fig. 14. Histograms of running times of the proposed method. (a) The stem mapping stage. (b) The stem matching stage. (c) The whole coarse registration process.

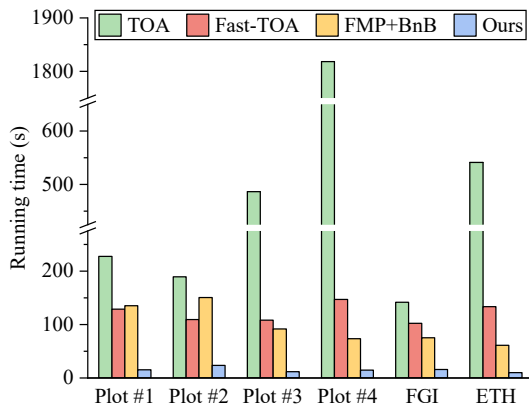


Fig. 15. Comparison of running times. Note that the running times of TOA and Fast-TOA contain only their stem matching part that performs on simplified stem maps ( $\sim 50$  trees/scan), and the times for the creation of their input (stem maps) were not included. For FMP+BnB, the running time includes both keypoint detection and matching, and similarly for our method, the running time includes both stem mapping and stem matching.

#### H. Limitation

Our stem mapping algorithm exploits cylinder primitives to extract tree stems, which may not handle tree stems with complex structures, e.g., tree stems consisting of multiple branches from the bottom (see Fig. 16). Since a large portion of real-world trees has a single main stem and the complex stems will be treated as outliers and filtered out in the global matching step, we have not encountered such issues in our experiments. However, our method will fail if the majority of

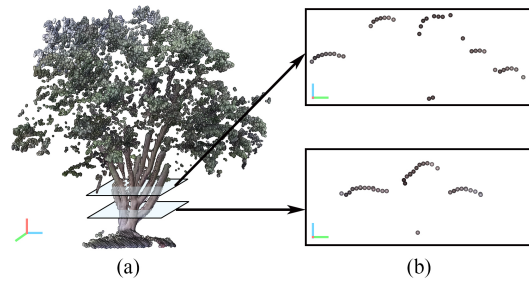


Fig. 16. A tree whose stem cannot be modeled using a cylinder. (a) Point cloud. (b) Two horizontal cross-sections of the point cloud.

the trees have such complex structures.

## VI. CONCLUSION

We have introduced an efficient and robust method to align TLS point clouds captured in forest environments. Our method accelerates the current stem-based registration strategy in both stages by proposing a fast stem mapping method as well as a robust and efficient stem matching algorithm requiring only the extracted stem positions. Compared to existing forest-oriented registration techniques, our method requires no additional tree attributes and enables fast stem matching, which resulted in significantly enhanced registration efficiency and robustness. We have also released a new benchmark dataset to the community to enable reliable evaluation and comparison of registration algorithms for forest point clouds.

Our method uses object-level primitives (i.e., tree stems) for registration, which has shown excellent performance. In future work, we would like to integrate this approach into frameworks for registration of multi-view data, co-registration of multi-platform data, and fusion of spatial-temporal data.

## REFERENCES

- [1] K. Calders, J. Adams, J. Armston, H. Bartholomeus, S. Bauwens, L. P. Bentley, J. Chave, F. M. Danson, M. Demol, M. Disney *et al.*, "Terrestrial laser scanning in forest ecology: Expanding the horizon," *Remote Sens. Environ.*, vol. 251, p. 112102, 2020.
- [2] M. Disney, "Terrestrial li dar: a three-dimensional revolution in how we look at trees," *New Phytol.*, vol. 222, no. 4, pp. 1736–1741, 2019.
- [3] X. Liang, V. Kankare, J. Hyypää, Y. Wang, A. Kukko, H. Haggren, X. Yu, H. Kaartinen, A. Jaakkola, F. Guan *et al.*, "Terrestrial laser scanning in forest inventories," *ISPRS J. Photogramm. Remote Sens.*, vol. 115, pp. 63–77, 2016.
- [4] Z. Cai, T.-J. Chin, A. P. Bustos, and K. Schindler, "Practical optimal registration of terrestrial lidar scan pairs," *ISPRS J. Photogramm. Remote Sens.*, vol. 147, pp. 118–131, 2019.
- [5] R. Huang, W. Yao, Y. Xu, Z. Ye, and U. Stilla, "Pairwise point cloud registration using graph matching and rotation-invariant features," *IEEE Geosci. Remote Sens. Lett.*, pp. 1–5, 2021.
- [6] S. Chen, L. Nan, R. Xia, J. Zhao, and P. Wonka, "Plade: A plane-based descriptor for point cloud registration with small overlap," *IEEE Trans. Geosci. Remote Sens.*, vol. 58, no. 4, pp. 2530–2540, 2019.
- [7] J. G. Henning and P. J. Radtke, "Detailed stem measurements of standing trees from ground-based scanning lidar," *For. Sci.*, vol. 52, no. 1, pp. 67–80, 2006.
- [8] J. G. Henning and P. J. Radtke, "Multiview range-image registration for forested scenes using explicitly-matched tie points estimated from natural surfaces," *ISPRS J. Photogramm. Remote Sens.*, vol. 63, no. 1, pp. 68–83, 2008.
- [9] X. Liang and J. Hyypää, "Automatic stem mapping by merging several terrestrial laser scans at the feature and decision levels," *Sensors*, vol. 13, no. 2, pp. 1614–1634, 2013.

- [10] J. Liu, X. Liang, J. Hyypää, X. Yu, M. Lehtomäki, J. Pyörälä, L. Zhu, Y. Wang, and R. Chen, "Automated matching of multiple terrestrial laser scans for stem mapping without the use of artificial references," *Int. J. Appl. Earth Obs. Geoinf.*, vol. 56, pp. 13–23, 2017.
- [11] D. Kelbe, J. Van Aardt, P. Romanczyk, M. Van Leeuwen, and K. Cawse-Nicholson, "Marker-free registration of forest terrestrial laser scanner data pairs with embedded confidence metrics," *IEEE Trans. Geosci. Remote Sens.*, vol. 54, no. 7, pp. 4314–4330, 2016.
- [12] D. Kelbe, J. Van Aardt, P. Romanczyk, M. Van Leeuwen, and K. Cawse-Nicholson, "Multiview marker-free registration of forest terrestrial laser scanner data with embedded confidence metrics," *IEEE Trans. Geosci. Remote Sens.*, vol. 55, no. 2, pp. 729–741, 2016.
- [13] J.-F. Tremblay and M. Béland, "Towards operational marker-free registration of terrestrial lidar data in forests," *ISPRS J. Photogramm. Remote Sens.*, vol. 146, pp. 430–435, 2018.
- [14] W. Dai, B. Yang, X. Liang, Z. Dong, R. Huang, Y. Wang, J. Pyörälä, and A. Kukko, "Fast registration of forest terrestrial laser scans using key points detected from crowns and stems," *Int. J. Digit. Earth*, vol. 13, no. 12, pp. 1585–1603, 2020.
- [15] X. Ge, Q. Zhu, L. Huang, S. Li, and S. Li, "Global registration of multiview unordered forest point clouds guided by common subgraphs," *IEEE Trans. Geosci. Remote Sens.*, 2021.
- [16] P. Polewski, W. Yao, L. Cao, and S. Gao, "Marker-free coregistration of uav and backpack lidar point clouds in forested areas," *ISPRS J. Photogramm. Remote Sens.*, vol. 147, pp. 307–318, 2019.
- [17] H. Guan, Y. Su, T. Hu, R. Wang, Q. Ma, Q. Yang, X. Sun, Y. Li, S. Jin, J. Zhang *et al.*, "A novel framework to automatically fuse multiplatform lidar data in forest environments based on tree locations," *IEEE Trans. Geosci. Remote Sens.*, vol. 58, no. 3, pp. 2165–2177, 2019.
- [18] M. Hauglin, V. Lien, E. Næsset, and T. Gobakken, "Geo-referencing forest field plots by co-registration of terrestrial and airborne laser scanning data," *Int. J. Remote Sens.*, vol. 35, no. 9, pp. 3135–3149, 2014.
- [19] A. Othmani, A. Piboule, M. Krebs, C. Stolz, and L. L. Y. Voon, "Towards automated and operational forest inventories with t-lidar," in *11th Int. Conf. LiDAR Appl. Assess. For. Ecosyst. (SilviLaser 2011)*, 2011.
- [20] X. Liang, P. Litkey, J. Hyypää, H. Kaartinen, M. Vastaranta, and M. Holopainen, "Automatic stem mapping using single-scan terrestrial laser scanning," *IEEE Trans. Geosci. Remote Sens.*, vol. 50, no. 2, pp. 661–670, 2011.
- [21] D. Kelbe, J. Van Aardt, P. Romanczyk, M. Van Leeuwen, and K. Cawse-Nicholson, "Single-scan stem reconstruction using low-resolution terrestrial laser scanner data," *IEEE J. Sel. Topics Appl. Earth Observ. Remote Sens.*, vol. 8, no. 7, pp. 3414–3427, 2015.
- [22] S. Xia, C. Wang, F. Pan, X. Xi, H. Zeng, and H. Liu, "Detecting stems in dense and homogeneous forest using single-scan tls," *Forests*, vol. 6, no. 11, pp. 3923–3945, 2015.
- [23] B. Yang, W. Dai, Z. Dong, and Y. Liu, "Automatic forest mapping at individual tree levels from terrestrial laser scanning point clouds with a hierarchical minimum cut method," *Remote Sens.*, vol. 8, no. 5, p. 372, 2016.
- [24] P. Polewski, W. Yao, M. Heurich, P. Krzystek, and U. Stilla, "A voting-based statistical cylinder detection framework applied to fallen tree mapping in terrestrial laser scanning point clouds," *ISPRS J. Photogramm. Remote Sens.*, vol. 129, pp. 118–130, 2017.
- [25] W. Ye, C. Qian, J. Tang, H. Liu, X. Fan, X. Liang, and H. Zhang, "Improved 3d stem mapping method and elliptic hypothesis-based dbh estimation from terrestrial laser scanning data," *Remote Sens.*, vol. 12, no. 3, p. 352, 2020.
- [26] W. Dai, B. Yang, X. Liang, Z. Dong, R. Huang, Y. Wang, and W. Li, "Automated fusion of forest airborne and terrestrial point clouds through canopy density analysis," *ISPRS J. Photogramm. Remote Sens.*, vol. 156, pp. 94–107, 2019.
- [27] H. Guan, Y. Su, X. Sun, G. Xu, W. Li, Q. Ma, X. Wu, J. Wu, L. Liu, and Q. Guo, "A marker-free method for registering multi-scan terrestrial laser scanning data in forest environments," *ISPRS J. Photogramm. Remote Sens.*, vol. 166, pp. 82–94, 2020.
- [28] B. Maiseli, Y. Gu, and H. Gao, "Recent developments and trends in point set registration methods," *J. Vis. Commun. Image Represent.*, vol. 46, pp. 95–106, 2017.
- [29] Z. Dong, F. Liang, B. Yang, Y. Xu, Y. Zang, J. Li, Y. Wang, W. Dai, H. Fan, J. Hyypää *et al.*, "Registration of large-scale terrestrial laser scanner point clouds: A review and benchmark," *ISPRS J. Photogramm. Remote Sens.*, vol. 163, pp. 327–342, 2020.
- [30] N. Haala, R. Reulke, M. Thies, and T. Aschoff, "Combination of terrestrial laser scanning with high resolution panoramic images for investigations in forest applications and tree species recognition," *Proceedings of the ISPRS working group V/1*, no. PART 5/W16, 2004.
- [31] P. Forsman and A. Halme, "3-d mapping of natural environments with trees by means of mobile perception," *IEEE Trans. Robot.*, vol. 21, no. 3, pp. 482–490, 2005.
- [32] M. Forsman, N. Börlin, and J. Holmgren, "Estimation of tree stem attributes using terrestrial photogrammetry," in *Int. Arch. Photogramm., Remote Sens. Spat. Inf. Sci. - ISPRS Arch.* Copernicus Gesellschaft, 2012, pp. B5–261.
- [33] D. Aiger, N. J. Mitra, and D. Cohen-Or, "4-points congruent sets for robust pairwise surface registration," in *ACM Trans. Graph.*, 2008, pp. 1–10.
- [34] X. Ge, "Automatic markerless registration of point clouds with semantic-keypoint-based 4-points congruent sets," *ISPRS J. Photogramm. Remote Sens.*, vol. 130, pp. 344–357, 2017.
- [35] P. J. Van Laarhoven and E. H. Aarts, "Simulated annealing," in *Simulated annealing: Theory and applications*. Springer, 1987, pp. 7–15.
- [36] A. Myronenko and X. Song, "Point set registration: Coherent point drift," *IEEE Trans. Pattern Anal. Mach. Intell.*, vol. 32, no. 12, pp. 2262–2275, 2010.
- [37] B. Zhao, X. Chen, X. Le, J. Xi, and Z. Jia, "A comprehensive performance evaluation of 3-d transformation estimation techniques in point cloud registration," *IEEE Trans. Instrum. Meas.*, vol. 70, pp. 1–14, 2021.
- [38] A. Gressin, C. Mallet, J. Demantké, and N. David, "Towards 3d lidar point cloud registration improvement using optimal neighborhood knowledge," *ISPRS J. Photogramm. Remote Sens.*, vol. 79, pp. 240–251, 2013.
- [39] H. Chen and B. Bhanu, "3d free-form object recognition in range images using local surface patches," *Pattern Recognit. Lett.*, vol. 28, no. 10, pp. 1252–1262, 2007.
- [40] A. Albarelli, E. Rodola, and A. Torsello, "A game-theoretic approach to fine surface registration without initial motion estimation," in *2010 IEEE Conf. Comput. Vis. Pattern Recognit. (CVPR)*. IEEE, 2010, pp. 430–437.
- [41] A. Aldoma, F. Tombari, L. Di Stefano, and M. Vincze, "A global hypotheses verification method for 3d object recognition," in *Eur. Conf. Comput. Vis. (ECCV)*. Springer, 2012, pp. 511–524.
- [42] B. Yang, Z. Dong, F. Liang, and Y. Liu, "Automatic registration of large-scale urban scene point clouds based on semantic feature points," *ISPRS J. Photogramm. Remote Sens.*, vol. 113, pp. 43–58, 2016.
- [43] A. S. Mian, M. Bennamoun, and R. Owens, "Three-dimensional model-based object recognition and segmentation in cluttered scenes," *IEEE Trans. Pattern Anal. Mach. Intell.*, vol. 28, no. 10, pp. 1584–1601, 2006.
- [44] P. W. Theiler, J. D. Wegner, and K. Schindler, "Globally consistent registration of terrestrial laser scans via graph optimization," *ISPRS J. Photogramm. Remote Sens.*, vol. 109, pp. 126–138, 2015.
- [45] J. Sanchez, F. Denis, P. Checchin, F. Dupont, and L. Trassoudaine, "Global registration of 3d lidar point clouds based on scene features: Application to structured environments," *Remote Sens.*, vol. 9, no. 10, p. 1014, 2017.
- [46] X. Liang, J. Hyypää, H. Kaartinen, M. Lehtomäki, J. Pyörälä, N. Pfeifer, M. Holopainen, G. Broly, P. Francesco, J. Hackenberg *et al.*, "International benchmarking of terrestrial laser scanning approaches for forest inventories," *ISPRS J. Photogramm. Remote Sens.*, vol. 144, pp. 137–179, 2018.
- [47] W. Zhang, J. Qi, P. Wan, H. Wang, D. Xie, X. Wang, and G. Yan, "An easy-to-use airborne lidar data filtering method based on cloth simulation," *Remote Sens.*, vol. 8, no. 6, p. 501, 2016.
- [48] J. Demantké, B. Vallet, and N. Paparoditis, "Streamed vertical rectangle detection in terrestrial laser scans for facade database production," in *ISPRS Ann. Photogramm. Remote Sens. Spat. Inf. Sci.*, vol. 1, no. September, 2012, pp. 99–104.
- [49] M. Weinmann, B. Jutzi, and C. Mallet, "Feature relevance assessment for the semantic interpretation of 3d point cloud data," *ISPRS Ann. Photogramm. Remote Sens. Spat. Inf. Sci.*, vol. 5, no. W2, p. 1, 2013.
- [50] J. Behley, V. Steinhage, and A. B. Cremers, "Efficient radius neighbor search in three-dimensional point clouds," in *2015 IEEE Int. Conf. Rob. Autom. (ICRA)*. IEEE, 2015, pp. 3625–3630.
- [51] J. Sanchez, F. Denis, D. Coeurjolly, F. Dupont, L. Trassoudaine, and P. Checchin, "Robust normal vector estimation in 3d point clouds through iterative principal component analysis," *ISPRS J. Photogramm. Remote Sens.*, vol. 163, pp. 18–35, 2020.
- [52] M. A. Fischler and R. C. Bolles, "Random sample consensus: a paradigm for model fitting with applications to image analysis and automated cartography," *Commun. ACM*, vol. 24, no. 6, pp. 381–395, 1981.

- [53] T. T. Pham, M. Eich, I. Reid, and G. Wyeth, "Geometrically consistent plane extraction for dense indoor 3d maps segmentation," in *2016 IEEE Int. Conf. Intell. Rob. Syst. (IROS)*. IEEE, 2016, pp. 4199–4204.
- [54] R. B. Rusu, W. Meeussen, S. Chitta, and M. Beetz, "Laser-based perception for door and handle identification," in *2009 Int. Conf. Adv. Rob. (ICAR)*. IEEE, 2009, pp. 1–8.
- [55] O. Sorkine-Hornung and M. Rabinovich, "Least-squares rigid motion using svd," *Computing*, vol. 1, no. 1, pp. 1–5, 2017.
- [56] B. PaulJ and M. NeilD, "A method for registration of 3-d shapes," *IEEE Trans. Pattern Anal. Mach. Intell.*, vol. 14, no. 2, pp. 239–256, 1992.
- [57] R. B. Rusu and S. Cousins, "3d is here: Point cloud library (pcl)," in *2011 IEEE Int. Conf. Rob. Autom. (ICRA)*. IEEE, 2011, pp. 1–4.
- [58] L. Dagum and R. Menon, "Openmp: an industry standard api for shared-memory programming," *IEEE Comput. Sci. Eng.*, vol. 5, no. 1, pp. 46–55, 1998.